


Three-body optical potentials in (d, p) reactions and their influence on indirect study of stellar nucleosynthesis

M. J. Dinmore, N. K. Timofeyuk, and J. S. Al-Khalili 

Department of Physics, Faculty of Engineering and Physical Sciences, University of Surrey, Guildford, Surrey, GU2 7XH, United Kingdom



(Received 17 June 2021; accepted 30 August 2021; published 10 September 2021)

Model uncertainties arising due to suppression of target excitations in the description of deuteron scattering and resulting in a modification of the two-body interactions in a three-body system are investigated for several (d, p) reactions serving as indirect tools for studying the astrophysical (p, γ) reactions relevant to rp process. The three-body nature of the deuteron-target potential is treated within the adiabatic distorted-wave approximation (ADWA) which relies on a dominant contribution from the components of the three-body deuteron-target wave function with small $n-p$ separations. This results in a simple prescription for treating the explicit energy dependence of two-body optical potentials in a three-body system requiring nucleon optical potentials to be evaluated at a shifted energy with respect to the standard value of half the deuteron incident energy. In addition, the ADWA allows for leading-order multiple-scattering effects to be estimated, which leads to a simple renormalization of the adiabatic potential's imaginary part by a factor of two. These effects are assessed using both nonlocal and local optical potential systematics for ^{26}Al , ^{30}P , ^{34}Cl , and ^{56}Ni targets at a deuteron incident energy of 12 MeV, which is typical for experiments with radioactive beams in inverse kinematics. The model uncertainties induced by the three-body nature of deuteron-target scattering are found to be within 40% both in the main peak of angular distributions and in total (d, p) cross sections. At higher deuteron energies, around 60 MeV, model uncertainties can reach 100% in the total cross sections. A few examples of application to astrophysically interesting proton resonances in ^{27}Si and ^{57}Cu obtained using (d, p) reactions and mirror symmetry are given.

DOI: [10.1103/PhysRevC.104.034614](https://doi.org/10.1103/PhysRevC.104.034614)

I. INTRODUCTION

To fully describe the relative abundances of the elements we must be able to properly constrain the reaction rates of the stellar processes that drive them. One class of reactions important for understanding stellar nucleosynthesis is proton capture, (p, γ) . Measuring (p, γ) cross sections directly is a difficult task since they are very small. One technique for the investigation of exotic nuclei produced by (p, γ) in stellar environments is to perform deuteron-induced one-nucleon transfer reactions (d, n) and (d, p) with radioactive beams, utilizing inverse kinematics. The first reaction, (d, n) , contains the same crucial piece of information—the overlap function of the wave functions of nuclei in initial and final states—as the (p, γ) reaction does. Populating bound states in (d, n) reactions provides these overlap functions in a straightforward manner. However, in many cases, such as the rp process, astrophysically important states are unbound, and their indirect access via the (d, n) reaction encounters problems both on the experimental side, where neutron detection could be problematic, and on the theoretical side, where the transfer to continuum is not yet well understood. The corresponding mirror states that could be populated in (d, p) reactions are bound and more easily accessible to study, both experimentally and theoretically. The information about widths Γ_p of proton states populated in (p, γ) reactions could be obtained

from the relations between these widths and the asymptotic normalization coefficients (ANCs) of their mirror states populated in (d, p) reactions [1]. The ANCs determine the magnitude of the asymptotic decrease of the overlap function.

Extracting ANCs from $A(d, p)B$ reactions takes place through comparison of measured angular distributions with those calculated with the help of reaction theory. Given that deuteron breakup effects are important, their effects are often accounted for in the adiabatic distorted-wave approximation (ADWA) [2]. This theory is based on a $n + p + A$ three-body description of the deuteron-target motion and involves pairwise $n-p$, $p-A$, and $n-A$ interactions. The latter two are assumed to be given by nucleon optical potentials taken at half the deuteron incident energy E_d . In reality, the $A + n + p$ system is a complex many-body system, and it was shown that projecting its wave function onto a three-body channel results in a complicated three-body optical operator that includes multiple scattering to all orders [3]. Even the simplest leading-order terms of this operator do not look like $n-A$ and $p-A$ optical potentials since they explicitly depend on the position of the third particle (p or n) and on the three-body rather than two-body energy. It has been possible to estimate the contribution of the leading terms of this operator within ADWA [3], which requires using nonlocal energy-dependent optical potentials taken at an energy shifted from the traditionally used value of $E_d/2$ by $n-p$ kinetic energy averaged over

the short range of the n - p force. Adding the first-order term of the three-body optical operator in a leading order results in a doubling of the dynamical part of this optical potential [4].

The present paper aims to quantify uncertainties, arising due to induced three-body force, of model predictions of (d, p) reactions used to indirectly probe (p, γ) capture that occurs in the rp process. We assess these effects within the ADWA. In Sec. II we summarize the ADWA three-body optical potential formalism of Refs. [3] and [4], arising due to neglecting the channels with target excitations. We apply this formalism to (d, p) reactions, listed in Sec. III, that could serve as indirect tools for measuring proton capture reactions of astrophysical interest. In Sec. IV we discuss numerical results obtained with different nucleon-nucleon (NN) models for a global nonlocal nucleon optical potential both with and without the induced leading-order multiple-scattering three-body force, and we also explore the possibility of using local optical potentials within this approach. In Sec. V we study model uncertainties due to the three-body optical potential in total (d, p) cross sections. In Sec. VI we apply mirror symmetry to determine the proton width of some astrophysically relevant states in ^{27}Si and ^{56}Co using their relations to the ANCs of their mirror states derived from (d, p) reactions. Conclusions are formulated in Sec. VII highlighting the necessity and directions for future research.

II. INDUCED THREE-BODY OPTICAL POTENTIALS WITHIN THE ADIABATIC DISTORTED-WAVE APPROXIMATION FORMALISM

It has been shown in Ref. [4] that projecting the many-body wave function of the $A + n + p$ system onto a three-body channel results in a three-body Hamiltonian

$$H_3 = T_3 + V_{np} + V_{\text{opt}}, \quad (1)$$

where T_3 is the three-body kinetic-energy operator, V_{np} is a short-range n - p interaction, and V_{opt} is a complicated three-body optical potential. The latter is the target-ground-state expectation value $\langle \phi_A | U | \phi_A \rangle$ of the optical operator U that contains multiple scattering to all orders:

$$U = \underbrace{U_{nA} + U_{pA}}_{U^{(0)}} + \underbrace{U_{nA} \frac{Q_A}{e} U_{pA} + U_{pA} \frac{Q_A}{e} U_{nA}}_{U^{(1)}} + \underbrace{U_{nA} \frac{Q_A}{e} U_{pA} \frac{Q_A}{e} U_{nA} + U_{pA} \frac{Q_A}{e} U_{nA} \frac{Q_A}{e} U_{pA} + \dots}_{U^{(2)}} \quad (2)$$

where

$$U_{NA} = \left(1 - v_{NA} \frac{Q_A}{e} \right)^{-1} v_{NA}. \quad (3)$$

Here, the operator Q_A projects onto the model space defined by all excited states of A and excluded from consideration, $e = E_3 + i0 - T_3 - V_{np} - (H_A - E_A)$, and E_3 is the three-body energy in the $A + n + p$ system, while v_{NA} is the sum of interactions of nucleon N (either n or p) with nucleons of the target A . The ground-state wave function ϕ_A is defined by the many-body Hamiltonian H_A , $H_A \phi_A = E_A \phi_A$, with E_A being the intrinsic binding energy of the target.

The ADWA model starts from expanding the eigenfunction $\Psi(\mathbf{R}, \mathbf{r})$ of the three-body Hamiltonian H_3 over the Weinberg basis functions $\phi_i(\mathbf{r})$,

$$[-\epsilon_d - T_r - \alpha_i V_{np}] \phi_i(\mathbf{r}) = 0, \quad i = 1, 2, \dots, \quad (4)$$

where \mathbf{r} is the n - p separation coordinate and T_r is the kinetic-energy operator associated with it. The ϕ_i satisfy the orthonormality relation

$$\langle \phi_i | V_{np} | \phi_j \rangle = -\delta_{i,j}. \quad (5)$$

The ADWA retains only the first term of the Weinberg-state expansion of $\Psi(\mathbf{R}, \mathbf{r})$ [2]. This results in the $\Psi(\mathbf{R}, \mathbf{r}) \approx \chi_{dA}^{(+)}(\mathbf{R}) \phi_d(\mathbf{r})$ approximation with ϕ_d being the deuteron ground-state wave function and the d - A channel distorted wave function $\chi_{dA}^{(+)}$ satisfying the two-body Schrödinger equation

$$[T_R + V^{\text{ADWA}}(\mathbf{R}) - E_d] \chi_{dA}^{(+)}(\mathbf{R}) = 0, \quad (6)$$

where T_R is the deuteron kinetic-energy operator associated with the relative coordinate \mathbf{R} connecting the centers of mass of the deuteron and the target A . The adiabatic potential V^{ADWA} is the first diagonal matrix element of the optical operator U , which due the Weinberg orthonormality condition is defined as $\langle \phi_1 | U | \phi_d \rangle$, where

$$\phi_1 = \frac{V_{np} \phi_d}{\langle \phi_d | V_{np} | \phi_d \rangle}. \quad (7)$$

The matrix element of the first term, $U^{(0)}$, of the operator U contains interactions of n and p with the target nucleons only, so that it can be associated with the n - A and p - A optical potentials. All other terms will contain interactions between n and p via excitation of excited states in A . The associated matrix elements will combine into a three-body potential. Including it into the model Hamiltonian will account for three-body effects induced by the target excitation. We call them induced three-body effects (I3B).

It has been shown in Ref. [4] that, in the ADWA, the simplest term, $U^{(0)} = U_{pA} + U_{nA}$, of the operator U is given by $U_{nA}^{\text{ADWA}} + U_{pA}^{\text{ADWA}}$, with

$$U_{NA}^{\text{ADWA}} = v_{NA} + v_{NA} \frac{Q_A}{E_{\text{eff}} - T_N - H_A - Q_A v_{NA} Q_A} v_{NA}, \quad (8)$$

where

$$E_{\text{eff}} = E_d/2 + \Delta E, \quad (9)$$

$$\Delta E = \frac{1}{2} \langle \phi_1 | T_{np} | \phi_d \rangle. \quad (10)$$

The representation (8) coincides with the definition of the N - A optical potential taken at energy E_{eff} equal to half the deuteron incident energy plus the n - p kinetic energy averaged over V_{np} [3]. The ADWA also allows the leading order of the term

$$U^{(1)} = U_{nA} \frac{Q_A}{e} U_{pA} + U_{pA} \frac{Q_A}{e} U_{nA} \quad (11)$$

to be evaluated. It was shown in Ref. [4] that

$$\langle \phi_1 \phi_A | U^{(0)} + U^{(1)} | \phi_A \phi_d \rangle \approx 2 \langle \phi_1 \phi_A | U^{(0)} | \phi_d \phi_A \rangle - \sum_{N=n,p} \langle \phi_1 \phi_A | v_{NA} | \phi_d \phi_A \rangle. \quad (12)$$

This has a simple connection with the nonlocal dispersive optical model (NLDM) potential given by

$$\begin{aligned} & \langle \phi_1 \phi_A | U^{(0)} + U^{(1)} | \phi_d \phi_A \rangle \\ & = V_{nA}^{HF} + 2\Delta V_{nA}^{dyn}(E) + V_{pA}^{HF} + 2\Delta V_{pA}^{dyn}(E), \quad (13) \end{aligned}$$

where V_{nA}^{HF} and $\Delta V_{nA}^{dyn}(E)$ are the Hartree-Fock and dynamical part, respectively. The latter contains an imaginary part, responsible for absorption, and a real part (or polarization potential) that contains contributions from all the excited states of A . Both V_{nA}^{HF} and $\Delta V_{nA}^{dyn}(E)$ are connected by dispersive relations [5]. Thus, induced three-body effects arising due to multiple scattering in the leading order can be accounted for by a simple doubling of the dynamic part of the optical potential.

The study involving $\langle \phi_1 \phi_A | U^{(0)} | \phi_d \phi_A \rangle$ only revealed that including energy dependence of the nonlocal optical potential via the energy shift ΔE can result in a significant difference from traditional $E_d/2$ -based ADWA calculations, and this result strongly depends on the assumptions about the energy dependence of the optical potentials [3,6]. In general, applying the energy shift gives higher (d, p) cross sections than those obtained in standard ADWA with local optical potentials. Including $\langle \phi_1 \phi_A | U^{(1)} | \phi_d \phi_A \rangle$ brings these cross sections down due to increased absorption [4]. Interestingly, with a stronger imaginary part increasing the dynamical real (polarization) part does not have any noticeable consequences for (d, p) cross sections. This justifies the use of phenomenological potentials that are not based on dispersive relations. This is important given that NLDM potentials are available for a very limited number of isotopes. Previous investigations have been carried out mainly for the $^{40}\text{Ca}(d, p)^{41}\text{Ca}$ reaction. Below we will concentrate on a few (d, p) reactions which are interesting from the point of view of indirect study of the astrophysical rp process.

III. (d, p) REACTIONS OF ASTROPHYSICAL INTEREST

Motivated by recent and ongoing experimental application of deuteron-induced one-nucleon transfer reactions to investigate stellar (p, γ) reaction rates we have selected four (d, p) reaction cases as indirect tools for astrophysical reaction studies. These reactions allow one to determine the spectroscopic information, the neutron spectroscopic factor, or the ANC associated with the overlap between the wave functions of the target and residual nucleus states. Using the mirror symmetry, discussed later in Sec. VI, one can find the corresponding protons spectroscopic information needed to calculate the proton radiative capture. The four selected reactions are the following.

- (i) $^{26}\text{Al}(d, p)^{27}\text{Al}$ as a surrogate for proton capture reaction $^{26}\text{Al}(p, \gamma)^{27}\text{Si}$, one of the major destruction pathways of ^{26}Al , primarily in Wolf Rayet stars, but also in AGB stars [7]. This capture reaction has been investigated with two indirect experimental methods using ^{26}Al beam, one measuring $^{26}\text{Al}(d, p)^{27}\text{Al}$ angular distributions [8,9] at an incident deuteron energy of $E_d = 12$ MeV and another measuring total

cross sections of $^{26}\text{Al}(d, n)^{27}\text{Si}$ [10] at $E_d = 60$ MeV. Both experiments have been performed to constrain the widths Γ_p of key ^{27}Si resonances.

- (ii) $^{30}\text{P}(d, p)^{31}\text{P}$ as a surrogate for $^{30}\text{P}(p, \gamma)^{31}\text{S}$ proton capture reactions, which are known to dominate the uncertainty in total abundances of sulfur isotopes [11], with the variation in reactions rates changing abundances by factors of up to 100 [12]. This uncertainty affects the abundances of nuclei that follow later in the rp process. There are no published experimental works that attempt this with (d, p) reactions but measurements of total cross sections using (d, n) reactions at $E_d = 60$ MeV to constrain ^{31}S resonances are reported in Ref. [13].
- (iii) $^{34}\text{Cl}(d, p)^{35}\text{Cl}$ as indirect probes for the $^{34}\text{Cl}(p, \gamma)^{35}\text{Ar}$ reaction, which contributes to the production of ^{35}Ar , an important isotopic observable in presolar grains in meteorites. The importance of uncertainties associated with this reaction on calculations of final abundances in oxygen neon novae has previously been highlighted [12], changing abundances of ^{34}S sevenfold, and the ability to reduce these uncertainties is of particular importance because the $^{32}\text{S}/^{34}\text{S}$ ratio is used to determine whether grains originate from novae [14]. New states in ^{35}Cl have been identified in $^{36}\text{Cl}(d, t)^{35}\text{Cl}$ reaction that include mirror analogs of astrophysical ^{35}Ar states [15], however, (d, t) experiments do not allow the partial proton widths Γ_p to be determined.
- (iv) $^{56}\text{Ni}(d, p)^{57}\text{Ni}$. In the late rp process and type-Ia supernovae, $^{56}\text{Ni}(p, \gamma)^{57}\text{Cu}$ reactions destroy the doubly magic $N = Z$ nucleus ^{56}Ni by populating resonances in ^{57}Cu [16,17]. Determining the production rate of the heavier than ^{56}Ni nuclei relies on ^{57}Cu resonance strengths and reaction rates of $^{56}\text{Ni}(p, \gamma)^{57}\text{Cu}$. They have been investigated with $^{56}\text{Ni}(d, p)^{57}\text{Ni}$ reactions using inverse kinematics, with experiments measuring differential cross sections carried out at an incident energy of $E_d = 8.9$ MeV [18], with integrated cross sections also having been measured at $E_d = 64$ MeV.

Each of these reactions will be investigated for a number of excited states, with a preference for states where experimental cross sections are available. The excitation energies and spin-parities of selected states probed for each reaction are listed in Table I.

All ADWA (d, p) calculations presented in this paper have been performed using the TWOFNR code [19], which has an option of reading externally generated distorted waves in and thus can easily accommodate any calculations with nonlocal potentials. When using nonlocal nucleon potentials in deuteron and proton channels we calculate the corresponding distorted waves as explained in Ref. [20]. All cross sections presented below are calculated in the zero-range approximation for $V_{np}(\mathbf{r})\phi_d(\mathbf{r}) \approx D_0\delta(\mathbf{r})$ in the (d, p) reaction T matrix, which is consistent with assumptions made in Refs. [3,4] to derive expressions (8), (11), and (12). The D_0 value does not depend on NN model choice, so we use a standard value

TABLE I. The ratio between the maximum of the differential cross sections peaks calculated at $E_d = 12$ MeV for reactions from the first column. The excitation energies (in keV), final-state spins, and quantum numbers of the populated level are given in the second, third, and fourth columns. The position of the maximum, θ , is given in the fifth column. In the following columns σ_{GRZ} and $\sigma_{\text{GRZ}}^{\text{I3B}}$ denote the cross sections calculated using GRZ without and with I3B, respectively, σ_{KD03} are standard Johnson-Tandy results with KD03 potentials, $\sigma_{\text{KD03}}^{\text{I3B}}$ are obtained by applying the shift ΔE and I3B effects to the local potential KD03, and $\sigma_{\text{KD03}}^{\text{NLE,I3B}}$ is obtained by restoring nonlocal equivalent of the local KD03 potential.

Reaction	E_x	J^π	lj	θ	$\sigma_{\text{GRZ}}/\sigma_{\text{KD03}}$	$\sigma_{\text{GRZ}}^{\text{I3B}}/\sigma_{\text{KD03}}$	$\sigma_{\text{GRZ}}^{\text{I3B}}/\sigma_{\text{GRZ}}$	$\sigma_{\text{KD03}}^{\text{I3B}}/\sigma_{\text{KD03}}$	$\sigma_{\text{KD03}}^{\text{NLE,I3B}}/\sigma_{\text{KD03}}$
$^{26}\text{Al}(d, p)^{27}\text{Al}$	3004	9/2 ⁺	$s_{\frac{1}{2}}$	0°	0.924	0.614	0.665	0.896	0.868
	7806	9/2 ⁺	$s_{\frac{1}{2}}$	0°	0.945	0.707	0.748	1.041	1.030
	7806	9/2 ⁺	$d_{\frac{3}{2}}$	22°	0.956	0.782	0.818	0.962	0.970
	7948	11/2 ⁻	$p_{\frac{1}{2}}$	13°	0.954	0.688	0.701	0.827	0.825
$^{30}\text{P}(d, p)^{31}\text{P}$	6336	1/2 ⁺	$s_{\frac{1}{2}}$	0°	0.989	0.736	0.744	1.046	1.036
	6336	1/2 ⁺	$d_{\frac{3}{2}}$	24°	1.018	0.807	0.793	0.992	0.997
	6399	7/2 ⁻	$f_{\frac{5}{2}}$	35°	1.208	0.812	0.673	0.907	0.907
$^{34}\text{Cl}(d, p)^{35}\text{Cl}$	6492	1/2 ⁺	$s_{\frac{1}{2}}$	0°	0.940	0.709	0.754	1.008	1.006
	6746	5/2 ⁺	$d_{\frac{5}{2}}$	24°	0.972	0.772	0.794	0.921	0.939
$^{56}\text{Ni}(d, p)^{57}\text{Ni}$	768	5/2 ⁻	$f_{\frac{5}{2}}$	34°	1.659	0.998	0.602	1.154	1.106
	1112	1/2 ⁻	$p_{\frac{1}{2}}$	15°	1.212	0.814	0.672	1.015	0.993
	2443	5/2 ⁻	$f_{\frac{5}{2}}$	35°	1.472	1.003	0.681	1.111	1.089
	2577	7/2 ⁻	$f_{\frac{7}{2}}$	35°	1.255	0.897	0.715	0.961	0.963

of $D_0 = -126.15$ MeV fm^{3/2}. The calculations are carried out with overlap integrals represented by single-particle wave functions calculated in a Woods-Saxon potential well with a radius $r_0 = 1.25$ fm, diffuseness $a = 0.65$ fm, and spin-orbit depth $V_{s.o.} = 6$ MeV. For the purposes of comparing different model calculations we employ the spectroscopic factor S equal to one.

IV. NUMERICAL RESULTS FOR ANGULAR DISTRIBUTIONS

A. Cross sections with different energy shift defined by deuteron model choice

We start with presenting calculations using global systematics of nonlocal optical potentials from Giannini, Ricco, and Zucchiatti (GRZ) [25]. This potential has energy-independent real part and energy-dependent imaginary part, which vanished at zero nucleon scattering energy and approaches exponentially to a constant value of 17.5 MeV with its increase. For this potential employing the shift ΔE is crucial since without it the imaginary part is too small to give sensible cross sections [3]. However, the numerical value of ΔE strongly depends on the choice of the NN interaction model, varying from 57 to 123 MeV [26]. Some of these values are shown in Table II. The n - p model choice for V_{np} in Eq. (1) also affects the ADWA solution for d - A distorted wave [26] so that we have two sources of NN -model-induced uncertainties when using energy-dependent nonlocal potentials.

To disentangle these uncertainties, we first fix V_{np} potential in the three-body Schrödinger equation choosing the Hulthén model [21], which results in using the Hulthén wave functions for ϕ_d and ϕ_1 in V^{ADWA} from Eq. (6), and make a series of calculations with GRZ potentials shifted by energies from 0 to 100 MeV with a step of 20 MeV. We have

chosen $^{26}\text{Al}(d, p)^{27}\text{Al}^*$ ($E_x = 7806$ keV) at $E_d = 12$ MeV as an example and studied it both for $l = 0$ and $l = 2$ orbital momentum transfer. Similar to what has been observed in Ref. [3], $\Delta E = 0$ leads to significantly higher cross sections in the main peak, however, for ΔE between 57 to 100 MeV, spanning most values generated by different NN models, the corresponding difference in angular distributions are small. This is explained by the fact that imaginary part of GRZ for $E > 60$ MeV is practically saturated and its energy dependence is very weak. Doubling the imaginary part according to prescription of Eq. (12) does not change this dependence.

As a next step, we used consistently the same NN model both in evaluating the shift ΔE and the functions ϕ_d and ϕ_1 that enter the matrix element $\langle \phi_1 | U^{(0)} + U^{(1)} | \phi_d \rangle$. We used four NN models, presented in Table II. The first of them, the Hulthén model, contains the deuteron s -wave state only. The other three models include contribution from the deuteron d -wave state. We account for this contribution exactly using approach developed in Ref. [20]. In Fig. 1 we show angular distributions for two (d, p) reactions populating mirror analogs of astrophysically relevant states, $^{26}\text{Al}(d, p)^{27}\text{Al}$ and $^{56}\text{Ni}(d, p)^{57}\text{Ni}$. The calculations are performed without and

TABLE II. ΔE values (in MeV) and percentage of d -state contribution for the different deuteron wave function models used.

Wave-function model	ΔE	D -state contribution
Hulthén [21]	57	0%
AV18 [22]	63.1	5.76%
CD-Bonn [23]	56.3	4.85%
χ EFT at N4LO with regulator of 0.8 fm [24]	123.6	4.29%

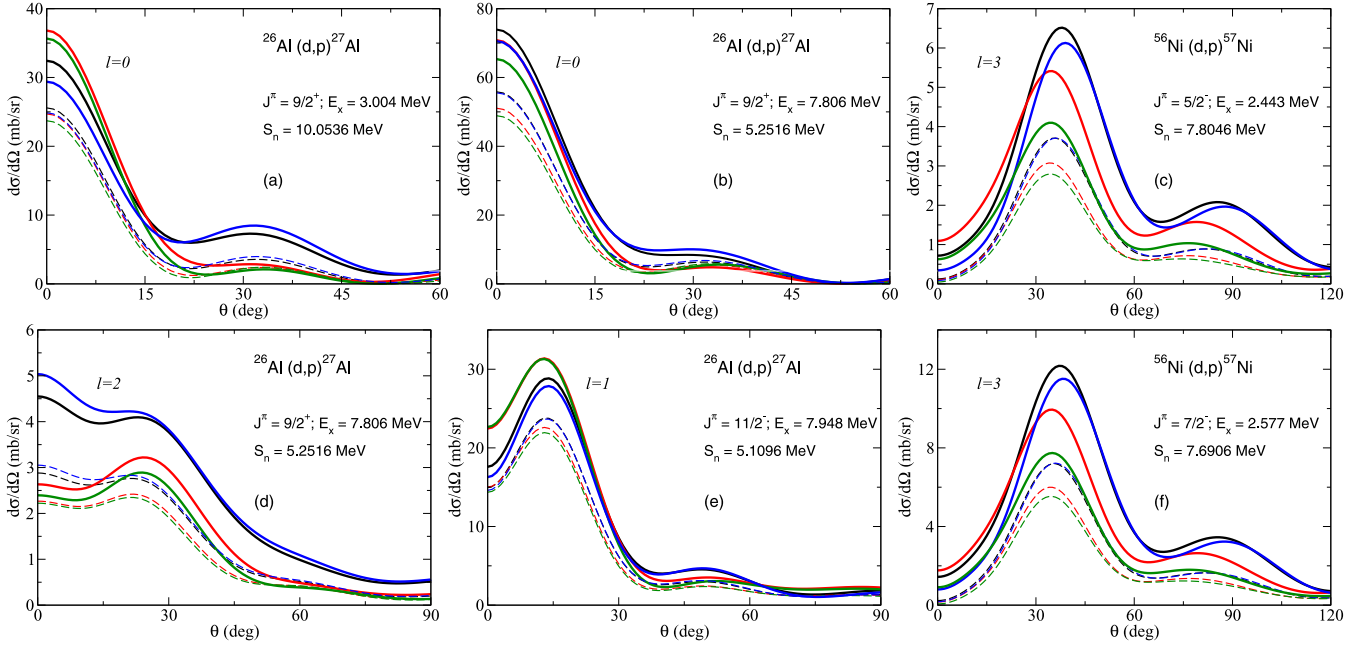


FIG. 1. Comparison of (a), (b), (d), (e) $^{26}\text{Al}(d, p)^{27}\text{Al}$ and (c), (f) $^{56}\text{Ni}(d, p)^{57}\text{Ni}$ cross sections calculated at $E_d = 12$ MeV with GRZ potentials with (dashed lines) and without (solid lines) I3B terms for NN models from Table II. The results with Hulthén, AV18, CD-Bonn, and χ EFT NN model choices are shown by green, black, red, and blue lines, respectively.

with doubling imaginary part of GRZ, which corresponds to the absence and presence of the I3B effects, respectively. The figure shows that without I3B effects the spread in the angular distributions due to different NN model choice is significant, up to 25% with respect to the average value for $l = 2$ and $l = 3$ transfers. This is similar to findings of Ref. [26] where energy-independent nonlocal potential was used. However, for the $l = 0$ and $l = 1$ cases the spread obtained with GRZ, around 5%–15% and although being smaller than that for $l = 2, 3$, is larger than that obtained in Ref. [26]. Also, in the case of the energy-independent nonlocal potential of Ref. [26], the cross sections in the main peak are clearly correlated with the matrix element $\langle \phi_1 | T_{np} | \phi_d \rangle$, being larger with increased values of the latter. This correlation seems to be either lost or not so well expressed for the energy-dependent potential GRZ when in some cases the cross sections for the smallest $\langle \phi_1 | T_{np} | \phi_d \rangle$ are the largest. This can be a result of small changes in the optical potential evaluated for different ΔE , when a smaller $\langle \phi_1 | T_{np} | \phi_d \rangle$ leads to a smaller imaginary part, which produces less absorption. When the I3B force is added, the spread between the cross sections obtained with different NN models is significantly reduced for all cases considered. It does not exceed 15% with respect to the average value for $l = 2, 3$ transfers, and is no larger than 10% for $l = 0$ and $l = 1$ transfers. Also, the correlation between $\langle \phi_1 | T_{np} | \phi_d \rangle$ is restored. Similar to findings of Ref. [4], the introduction of I3B significantly lowers the cross sections. We have performed calculations (not shown here) for two other reactions including sd -shell targets ^{30}P and ^{34}Cl at the same deuteron incident energy of 12 MeV and populating the ^{31}P and ^{35}Cl states from Table I. We came to the same conclusions about I3B effects and NN model choice as in the case of ^{26}Al and ^{56}Ni .

B. Nonlocal optical potential and deuteron s -wave model

The strong dependence of ΔE on NN model arises in ADWA mainly due to including a deuteron d state in ϕ_1 [20,26], which opens the door to a large contribution from poorly known high- n - p momenta into $\langle \phi_1 | T_{np} | \phi_d \rangle$. Such a contribution also affects the ADWA d - A scattering waves and (d, p) cross sections, obtained with nonlocal optical potentials, which is a drawback of ADWA that should disappear when three-body $A + n + p$ dynamics is treated exactly [27,28]. However, if only the s -wave state is retained in the deuteron wave function then the contribution to ΔE is dominated by low- n - p momentum physics where sensitivity to the n - p model is weak. In the rest of the paper we choose the Hulthén model for V_{np} , ϕ_d , ϕ_1 , and ΔE . As shown in Ref. [28], in this case ADWA with nonlocal energy-independent potentials gives (d, p) results that are closer to those obtained in exact three-body calculations.

We have calculated angular distributions for reactions from Table I using the GRZ potential evaluated for $\Delta E = 57$ MeV without and with I3B force. We compare them to the standard Johnson-Tandy ADWA cross sections obtained with local optical potential KD03 [29]. These calculations have been carried out for an incident deuteron energy of 12 MeV available at several radioactive beam facilities. We have discovered that without the I3B force the main peak cross sections σ_{KD03} and σ_{GRZ} , obtained with GRZ and KD03, respectively, are very similar for populating ^{27}Al , $^{31}\text{P}^*(6336)$, and ^{35}Cl excited states. Their ratio is shown in Table I. In the case of $^{31}\text{P}^*(6336)$ and ^{57}Ni final states, σ_{GRZ} is larger than σ_{KD03} by 20%–66%. A few selected angular distributions for populating $1s$, $0d$, $1p$, and $0f$ states are shown in Fig. 2. One can see that including an energy shift does not change the shape of

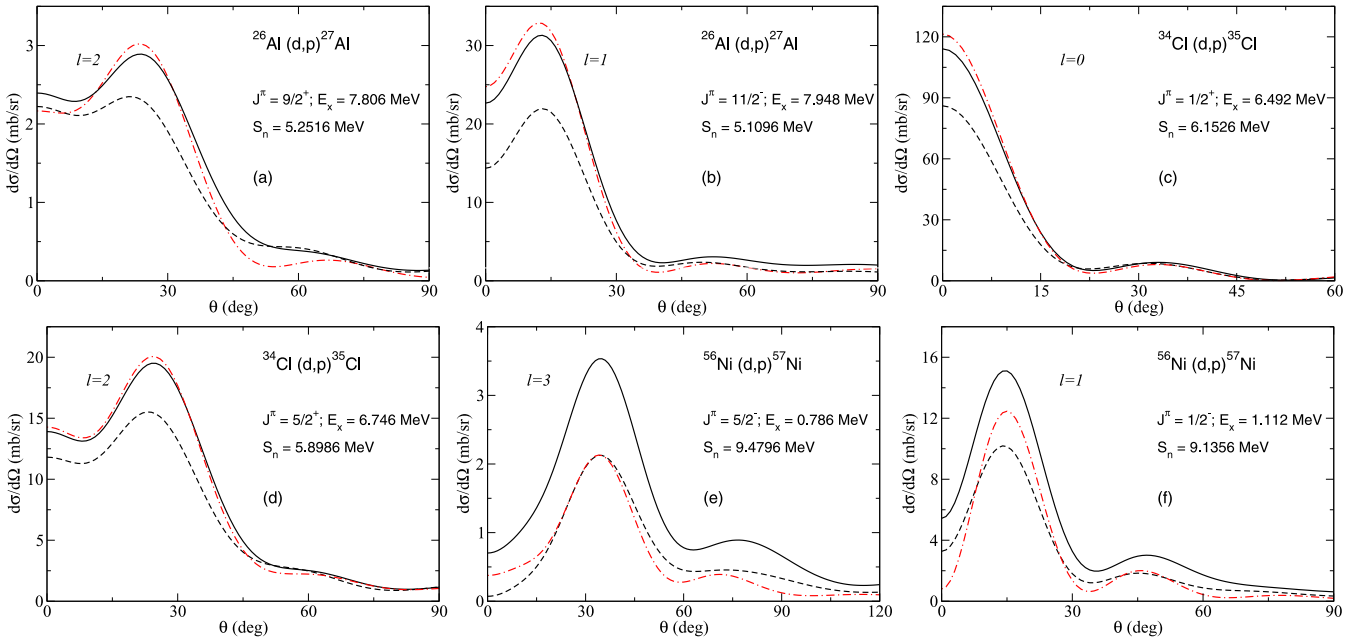


FIG. 2. The ADWA angular distributions for (a), (b) $^{26}\text{Al}(d, p)$; (c), (d) $^{34}\text{Cl}(d, p)$; and (e), (f) $^{56}\text{Ni}(d, p)$ reactions and populating (c) $l = 0$; (b), (f) $l = 1$; (a), (d) $l = 2$; and (e) $l = 3$ states calculated at $E_d = 12$ MeV using the nonlocal GRZ potential with (dashed) and without (solid) I3B terms in comparison with those obtained using standard Johnson-Tandy model with the local KD03 potential (dot-dashed).

angular distributions very much, resulting mainly in the renormalization of the cross sections. Including I3B force leads to decrease of the peak cross section by 60%–80% as shown in Table I by ratios $\sigma_{\text{GRZ}}^{13\text{B}}/\sigma_{\text{GRZ}}$. As the result, in most of the peak cross sections with GRZ and I3B force are much smaller than those obtained with KD03, only a few cases being within 10% of the KD03 results.

The ratios $\sigma_{\text{GRZ}}^{13\text{B}}/\sigma_{\text{KD03}}$ indicate how much the spectroscopic factors change if the GRZ + I3B model is used instead of the ADWA with KD03. If these spectroscopic factors are used for (p, γ) determination then the corresponding model uncertainty will propagate to the proton capture cross sections in similar proportions.

C. Local global systematics

Most global systematics of optical potentials are local. It is therefore of interest to check the consequences of applying an adiabatic model of three-body optical potentials for the case of local potentials. We have chosen the KD03 systematics for n - A and p - A potentials, which were evaluated at $E_{\text{eff}} = E_d/2 + \Delta E$ with $\Delta E = 57$ MeV to account for energy dependence of optical potentials and then multiplied their imaginary parts by the factor of two. To gauge the impact of these modifications to N - A potentials we compare the results obtained with those from the standard Johnson-Tandy ADWA approach employing the same KD03 potential but without any modifications.

We found that the reduction in the real part of deuteron-target adiabatic potentials that results from the inclusion of ΔE (roughly 15 MeV for the cases we investigate) produces a notable increase in the cross section. This is comparable in magnitude to the reduction caused by the addition of I3B

terms. Some states display a greater sensitivity to the additions, with their impact most obvious for Ni calculations, but in general it was found that the reduction in cross section caused by the doubling of the imaginary potential offsets the effects of the energy shift. This is demonstrated in Fig. 3 for a few typical cases. The factors that these cross sections differ by are denoted as $\sigma_{\text{KD03}}^{13\text{B}}/\sigma_{\text{KD03}}$ and shown in Table I. They can be as large as 25%, while most fall within 5% of cross sections generated using a standard approach, with little to no change found in the angular distribution.

It is known that local and nonlocal optical potentials give similar description of nucleon elastic scattering if the following transformation between the nonlocal potential and its local equivalent U_{loc}^N is used [30],

$$U_{\text{loc}}^N(r) = U_{NA}(r) \exp \left\{ \frac{\mu \beta^2}{2\hbar^2} [U_{\text{loc}}^N(r) - \bar{V}_c] \right\}, \quad (14)$$

where μ is the N - A reduced mass and \bar{V}_c is the Coulomb potential. This transformation assumes that the optical potentials are of the Perey-Buck form [30]:

$$\tilde{U}_{NA}(E, r, r') = H(|r - r'|) U_{NA} \left(E, \frac{r + r'}{2} \right), \quad (15)$$

where $H(x) = \pi^{-3/2} \beta^{-3} \exp(-x^2/\beta^2)$ and β is some nonlocality range. A few recent examples of how this transformation performs and references to more literature on this subject can be found in Ref. [31]. We can assume that a known phenomenological energy-dependent optical potential $U_{\text{phen}}(E, r)$ is a local-equivalent analog of an underlying nonlocal energy-dependent potential $\tilde{U}_{NA}(E, r, r')$, which we can restore through the transformation (14). Then, according to Sec. II one should use form factors $U_{NA}(E, r)$ taken at the

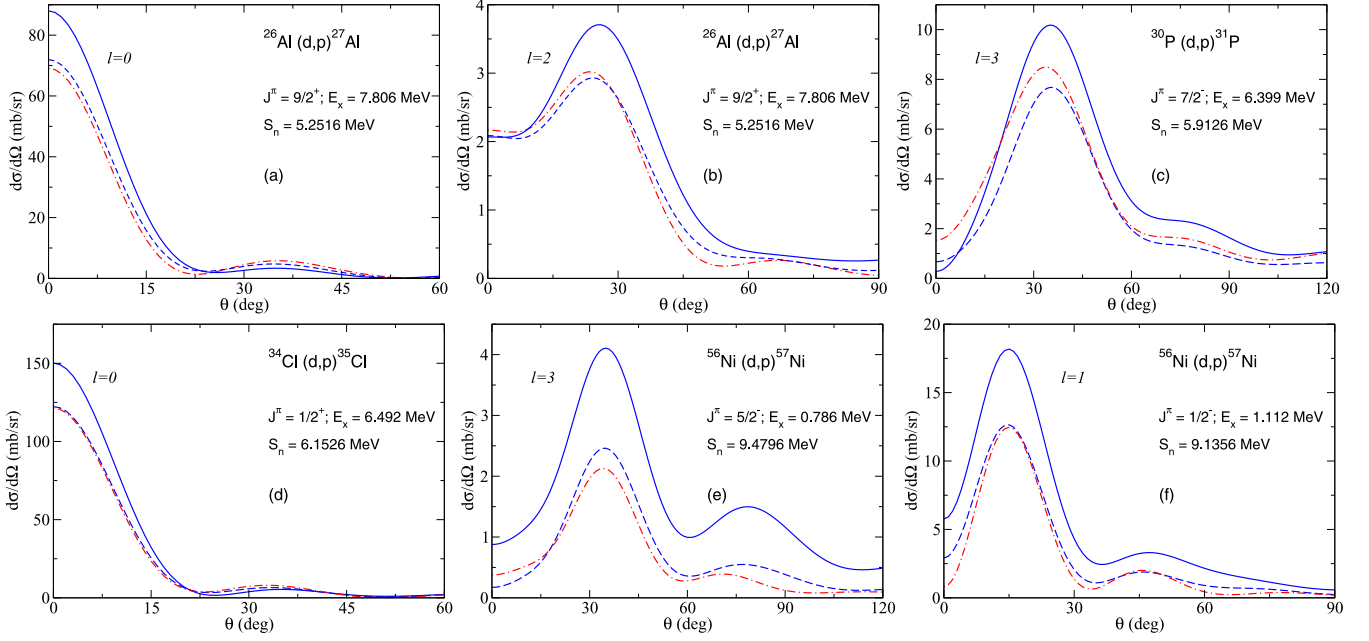


FIG. 3. The ADWA angular distributions for (a), (b) $^{26}\text{Al}(d, p)$; (c) $^{30}\text{P}(d, p)$; (d) $^{34}\text{Cl}(d, p)$; and (e), (f) $^{56}\text{Ni}(d, p)$ reactions and populating (a), (d) $l=0$; (f) $l=1$; (b) $l=2$; and (c), (e) $l=3$ states calculated at $E_d = 12$ MeV using the KD03 potential evaluated at a shifted by 57 MeV energy with (dashed) and without (solid) I3B terms in comparison with those obtained using standard Johnson-Tandy model with the same KD03 potential (dot-dashed).

energy $E = E_{\text{eff}} = E_d/2 + \Delta E$, treating them as energy independent. It was shown in Ref. [3] that this results in the local d - A distorting potential U_{loc} being used in (d, p) calculations, which is obtained from the transcendental equation

$$U_{\text{loc}}(E_d, r) \exp \left[-\frac{\mu_d \beta_d^2}{2\hbar^2} U_{\text{loc}}(E_d, r) \right] = \mathcal{V}(E_d, r), \quad (16)$$

where

$$\begin{aligned} \mathcal{V}(E_d, r) &= \exp \left[\frac{\mu \beta^2}{2\hbar^2} E_{\text{eff}} - \frac{\mu_d \beta_d^2}{2\hbar^2} (E_d - \bar{V}_c) \right] \\ &\times M_0 \left[U_{\text{phen}}^n(E_{\text{eff}}, r) \exp \left[-\frac{\mu \beta^2}{2\hbar^2} U_{\text{phen}}^n(E_{\text{eff}}, r) \right] \right. \\ &\left. + U_{\text{phen}}^p(E_{\text{eff}}, r) \exp \left[-\frac{\mu \beta^2}{2\hbar^2} (U_{\text{phen}}^p(E_{\text{eff}}, r) - \bar{V}_c) \right] \right]. \end{aligned} \quad (17)$$

Here μ_d is the d - A reduced mass, M_0 is the value that quantifies the overlap of ϕ_1 , modified by nonlocality, with ϕ_d and β_d is the deuteron effective nonlocality range. Exact definitions of M_0 and β_d can be found in Ref. [32].

We use the KD03 potential as U_{phen}^N and assume a standard value for the nonlocality range $\beta = 0.85$ fm, which in the Hulthén model gives $M_0 = 0.78$ and $\beta_d = 0.4$ fm [32]. We calculate U_{loc} from Eqs. (16) and (17) and use it in local (d, p) calculations for the targets of previous sections and compare the outcome with standard Johnson-Tandy KD03 calculations. A few typical angular distributions are shown in Fig. 4. We have found that the angular distributions populating final s -,

p -, and d -wave states calculated with U_{loc} are very similar to those obtained by directly applying the shift and I3B to the local KD03 potential with some differences seen for the cross sections to final f -wave state. In general, the differences increase with the orbital momenta of the transferred neutron. The ratios $\sigma_{\text{KD03}}^{\text{NLE, I3B}} / \sigma_{\text{KD03}}$ of the cross sections in the maximum, obtained using these two different approaches employing local optical potentials systematics, are shown in Table I. Most results obtained with the two methods agrees within 3%, the largest difference being 6% for $^{57}\text{Ni}(768 \text{ keV})$ state.

V. MODEL UNCERTAINTIES IN TOTAL (d, p) CROSS SECTIONS

Usually, the determination of ANCs relies on a theoretical description of the angular distribution within the main maximum where the direct peripheral transfer mechanism is dominant. However, in some inverse-kinematics-based experiments with radioactive beams this is not always possible. For example, detecting neutrons from (d, n) reactions that could probe Γ_p directly can be very difficult. Also, deducing (d, n) angular distributions by detecting the charged products of the resonance decay in coincidence could be very challenging due to the necessity of collecting a large proportion of resulting protons, having a good energy calibration and an absence of any contamination in the beam. For very narrow proton resonances of astrophysical interest lying close to the proton threshold, where γ -decay mode dominates, it has been possible to measure the total cross sections for a population of excited final states by detecting γ rays emitted in their deexcitation (see, for example, Refs. [10, 13]). Total cross sections

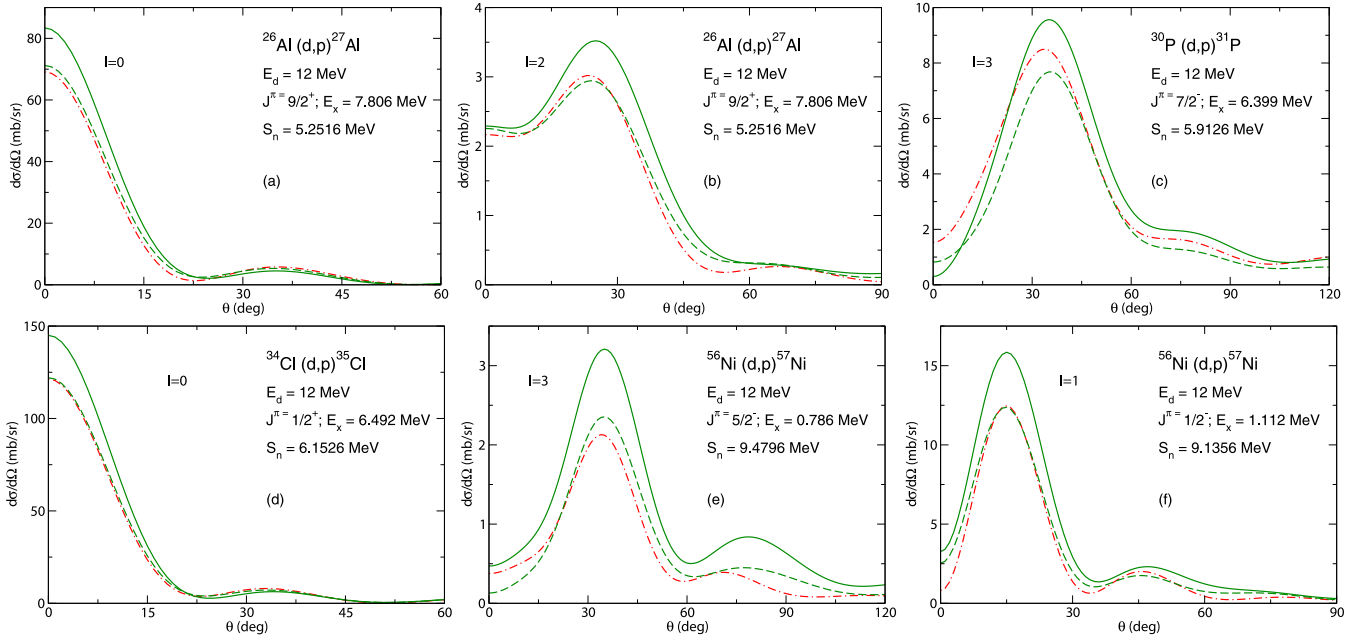


FIG. 4. The ADWA angular distributions for (a), (b) $^{26}\text{Al}(d,p)^{27}\text{Al}$; (c) $^{30}\text{P}(d,p)^{31}\text{P}$; (d) $^{34}\text{Cl}(d,p)^{35}\text{Cl}$; and (e), (f) $^{56}\text{Ni}(d,p)^{57}\text{Ni}$ reactions and populating (a), (d) $l=0$; (f) $l=1$; (b) $l=2$; and (c), (e) $l=3$ states calculated at $E_d = 12$ MeV using the nonlocal equivalent of the KD03 potential with (dashed) and without (solid) I3B terms in comparison with those obtained using standard Johnson-Tandy model with the same KD03 potential (dot-dashed).

only were also measured in some (d,p) experiments [33,34] without the corresponding differential cross sections.

The differential cross section at the main peak and the total cross section may carry different physical information. Indeed, the latter are obtained as

$$\sigma = \int_0^{2\pi} d\varphi \int_0^\pi \frac{d\sigma(\theta)}{d\Omega} \sin\theta d\theta, \quad (18)$$

which contain $\sin\theta$ that suppresses the contribution from forward angles.

This suppression could be particularly relevant for population of s -wave final nucleon states, most interesting in astrophysical applications, especially for higher incident energies. Increased contribution from a wider angular range, where other mechanisms may come into play and where peripherality may be lost, can lead to larger model uncertainties in the total cross sections than those established in the main peak.

In Table III we show the various ratios of total (d,p) cross sections calculated in the same models that were used to obtain the results presented in Table I. We show these ratios for two typical deuteron energies, $E_d = 12$ MeV, already studied in previous sections and often used for measuring differential cross sections, and $E_d = 60$ MeV, which has been used several times to measure the total cross sections for (d,n) reactions.

For $E_d = 12$ MeV, the difference between the total $\sigma_{\text{GRZ}}^{13\text{B}}$ and σ_{KD03} cross sections is within 30%. Unlike in the case of ratios of peak cross sections, where $\sigma_{\text{GRZ}}^{13\text{B}}$ are either lower or similar to σ_{KD03} , the total cross section of $\sigma_{\text{GRZ}}^{13\text{B}}$ could be either larger or smaller than those of σ_{KD03} ones. The ratios $\sigma_{\text{GRZ}}^{13\text{B}}/\sigma_{\text{KD03}}$ of total cross sections are larger than the corresponding ratios of peak cross sections, thus confirming that

the model uncertainties in the total cross sections are generally higher than those in the peak values. Similar situation occurs when local potential KD03, modified to account for three-body effects, is used in calculations. Different treatment of this modification, either applied directly or using local potential reconstruction technique of Eqs. (16) and (17) via nonlocal equivalent of KD03, gives the total cross sections differing by no more 6%, which is marginally larger than the difference of 2% between that obtained by the two methods for peak cross sections.

The calculations at $E_d = 60$ MeV revealed that the cross sections are much more sensitive to the model choice for V_{np} , to extent that this choice can strongly affect the shapes of the angular distributions (not shown here). Similar effect has been observed in Ref. [28] for $^{26m}\text{Al}(d,p)^{27}\text{Al}$ at $E_d = 50$ MeV. As in previous sections, we use the Hulthén model, which in the case of nonlocal potentials suppresses the contribution from poorly defined high n - p momenta causing strong deviation of the ADWA cross sections from exact three-body dynamics predictions. Unlike in the case of $E_d = 12$ MeV, applying the energy shift and doubling imaginary part can dramatically affect the shapes of angular distributions so that they may lose resemblance with the standard ADWA predictions. Significant shape changes make comparison of peak cross sections meaningless. We calculate the ratio of the total cross sections obtained with ΔE and I3B force to the standard ADWA ones showing them in Table III. As in the case of $E_d = 12$ MeV, we apply the shift ΔE and doubling imaginary part to nonlocal potential GRZ and to local potential KD03, both directly or to its nonlocal equivalent. The three-body effects introduced in this way have a stronger influence on the total cross sections than in the 12 MeV case, in particular for populating $s_{1/2}$

TABLE III. Ratio between total cross sections peaks calculated from the first column at deuteron energies given in the fifth column. The excitation energies (in keV), final-state spins, and quantum numbers of the populated level are given in the second, third, and fourth columns. In the following columns σ_{GRZ} and $\sigma_{\text{GRZ}}^{\text{I3B}}$ denote the cross sections calculated using GRZ without and with I3B, respectively, σ_{KD03} are standard Johnson-Tandy results with KD03 potentials, $\sigma_{\text{KD03}}^{\text{I3B}}$ are obtained by applying the shift ΔE and I3B effects to the local potential KD03, and $\sigma_{\text{KD03}}^{\text{NLE,I3B}}$ is obtained by restoring nonlocal equivalent of the local KD03 potential.

Reaction	E_x	J^π	lj	E_d (MeV)	$\sigma_{\text{GRZ}}^{\text{I3B}}/\sigma_{\text{KD03}}$	$\sigma_{\text{KD03}}^{\text{I3B}}/\sigma_{\text{KD03}}$	$\sigma_{\text{KD03}}^{\text{NLE,I3B}}/\sigma_{\text{KD03}}$	
$^{26}\text{Al}(d, p)^{27}\text{Al}$	3004	$9/2^+$	$s_{\frac{1}{2}}$	12	0.886	1.187	1.169	
				60	0.725	1.112	1.239	
	7806	$9/2^+$	$s_{\frac{1}{2}}$	12	0.990	1.078	1.106	
				60	1.579	1.725	2.075	
	7806	$9/2^+$	$d_{\frac{3}{2}}$	12	1.027	1.180	1.187	
				60	0.557	1.013	1.073	
	7948	$11/2^-$	$p_{\frac{1}{2}}$	12	0.745	0.817	0.804	
				60	0.458	0.623	0.640	
$^{30}\text{P}(d, p)^{31}\text{P}$	6336	$1/2^+$	$s_{\frac{1}{2}}$	12	0.959	1.013	1.044	
				60	1.712	1.765	2.137	
	6336	$1/2^+$	$d_{\frac{3}{2}}$	12	1.068	1.155	1.173	
				60	0.654	1.101	1.178	
	6399	$7/2^-$	$f_{\frac{5}{2}}$	12	0.823	0.836	0.838	
				60	0.471	0.759	0.721	
	$^{34}\text{Cl}(d, p)^{35}\text{Cl}$	6492	$1/2^+$	$s_{\frac{1}{2}}$	12	0.902	0.956	0.989
					60	1.833	1.718	2.088
6746		$5/2^+$	$d_{\frac{5}{2}}$	12	0.857	0.867	0.906	
				60	0.921	1.184	1.265	
$^{56}\text{Ni}(d, p)^{57}\text{Ni}$		768	$5/2^-$	$f_{\frac{5}{2}}$	12	1.244	1.352	1.258
					60	0.522	0.851	0.824
		1112	$1/2^-$	$p_{\frac{1}{2}}$	12	1.126	1.231	1.165
					60	1.050	1.089	1.188
	2443	$5/2^-$	$f_{\frac{5}{2}}$	12	1.300	1.340	1.285	
				60	0.628	0.950	0.935	
	2577	$7/2^-$	$f_{\frac{7}{2}}$	12	1.065	1.029	1.026	
				60	0.935	1.167	1.164	

states, as expected. This influence is different depending of what kind of potential was used in the calculations, nonlocal GRZ or local KD03 corrected for I3B effects. In general, the model uncertainty due to the three-body nature of optical potentials can be as large as a factor of two. It can result both in an increase and a decrease of the cross sections depending on the reaction choice.

VI. NEUTRON ASYMPTOTIC NORMALIZATION COEFFICIENTS AND PROTON WIDTHS OF MIRROR STATES

To illustrate how model uncertainties due to three-body nature of optical potentials in the $A + n + p$ system affect information about reactions in stellar environments, we have determined ANC's for $^{27}\text{Al}^*(7806, 7948)$ and $^{57}\text{Ni}^*(768, 1112)$ states from the (d, p) angular distributions measured at $E_d = 12$ and 8.9 MeV in Refs. [9] and [18], respectively, and then calculated the widths of mirror proton resonances using the relation [1]

$$\frac{\Gamma_p}{C_n^2} \approx \mathcal{R}_{\text{res}} \equiv \frac{\kappa_p}{\mu} \left| \frac{F_l(\kappa_p R_N)}{\kappa_p R_N j_l(i\kappa_n R_N)} \right|^2, \quad (19)$$

where C_n is the neutron ANC, $\kappa_{(n,p)} = (2\mu\varepsilon_{(n,p)}/\hbar^2)^{1/2}$, μ is the A - N reduced mass, $\varepsilon_{(n,p)}$ is the (positive) separation for neutron or proton resonance energy, $R_N = R_0 A^{1/3}$ is the range of internal region of A , j_l is a spherical Bessel function, and F_l is the regular Coulomb wave function. We have chosen $R_0 = 1.3$ fm and checked that for all our cases the ratio \mathcal{R}_{res} changes by less than 2% for $1.25 \leq R_0 \leq 1.35$ fm. We should note that Eq. (19) is a model-independent approximation suitable for fast calculations because it requires knowledge of nucleon energies and target charges only. Since we investigate the dependence of neutron ANCs and mirror proton widths on optical potentials only, for the purpose of our paper, the exact value of Γ_p/C_n^2 is not needed. However, it can be obtained in terms of the Wronskians from the radial overlap functions and regular solutions of the two-body Schrödinger equation with the short-range interaction excluded (see Ref. [35] for details).

We first checked the extent to which the chosen reactions are peripheral by changing the radius r_0 of the bound neutron potential within the range of 1.1–1.4 fm and comparing the calculated cross sections to the experimental ones. In all cases the spectroscopic factors changed much more strongly than the ANCs with varying r_0 , which is a good indication that the reactions considered are mainly sensitive to the peripheral

TABLE IV. Squared ANC's C_n^2 (in fm⁻¹) and widths Γ_p (in eV) for mirror pairs shown in first column. The second and third columns display resonance energies E_R (in MeV) and nucleon orbital momentum l . The calculations are shown for standard ADWA with KD03 (fourth and fifth columns) and for I3B effects included in nonlocal GRZ and local KD03 optical potentials. The I3B effect in the latter was introduced either directly (eighth and ninth columns) or in its nonlocal equivalent (tenth and eleventh columns).

Mirror pair	E_R	l	KD03		GRZ + I3B		KD03(L) + I3B		KD03(NLE) + I3B	
			C_n^2	Γ_p	C_n^2	Γ_p	C_n^2	Γ_p	C_n^2	Γ_p
²⁷ Al(7806)- ²⁷ Si(7590)	127	0	0.258	6.27×10^{-8}	0.365	8.88×10^{-8}	0.247	6.01×10^{-8}	0.250	6.08×10^{-8}
²⁷ Al(7806)- ²⁷ Si(7590)	127	2	0.148	2.15×10^{-9}	0.128	1.86×10^{-9}	0.125	1.81×10^{-9}	0.120	1.74×10^{-9}
²⁷ Al(7948)- ²⁷ Si(7652)	189	1	0.650	3.63×10^{-5}	0.979	5.47×10^{-5}	0.793	4.43×10^{-5}	0.797	4.45×10^{-5}
⁵⁷ Ni(768)- ⁵⁷ Cu(1028)	336	3	23.2	1.24×10^{-11}	15.2	8.14×10^{-12}	18.9	1.01×10^{-11}	19.8	1.06×10^{-11}
⁵⁷ Ni(1112)- ⁵⁷ Cu(1106)	416	1	202	2.64×10^{-7}	163	2.13×10^{-7}	203	2.65×10^{-7}	203	2.65×10^{-7}

region of the nucleus. The strongest spread in ANC squared, up to 14%, was observed for populating ⁵⁷Ni*(1112). However, in this case the spectroscopic factor changed by 43% with respect to the value obtained with standard radius $r_0 = 1.25$ fm. Since our main aim is to quantify uncertainties due to the I3B effects, we ignore the uncertainties in ANC's due to residual dependence on r_0 as well as experimental uncertainties. We note that for the ²⁷Al(7806) state the cross section is a sum of two terms corresponding to $l = 0$ and $l = 2$ transfers. This creates additional uncertainties for ANC's determined for this particular state.

The ANC's squared, proton widths of mirror states for GRZ, and two versions of corrected KD03 potential are shown in Table IV. Results obtained with standard ADWA employing the same KD03 are shown there as well. One can see that introducing I3B effects gives different results depending on nuclear state and on what kind of potential is employed, local or nonlocal. The I3B effect can work both ways, either increasing or decreasing C_n^2 and the corresponding Γ_p values, in the worst case—⁵⁷Ni(768) state with GRZ—deviating from the standard ADWA approach by 52%. Accounting for I3B force using local optical potential KD03 in most cases does not exceed 22% change with respect to ADWA, apart from the $l = 2$ case in ²⁶Al(7806) where the uncertainty of extracted C_n^2 is expected to be large. In all cases the two different ways of introducing I3B effects based on KD03 local potential give very similar results. Introducing I3B force into nonlocal potential GRZ can cause a stronger effect, up to 52% in ⁵⁷Ni(1112).

The widths Γ_p shown in Table IV have already been determined using mirror-symmetry assumptions in previous works from (d, p) angular distributions [9,18]. But these widths were estimated using a different model which assumes that Γ_p is given by the product of the Coulomb-barrier penetrability factor, the doubled Wigner single-particle width, and the proton spectroscopic factor, equal to that of the mirror neutron. While the assumption about equality of spectroscopic factors in mirror states should be good, the Coulomb-barrier penetrability depends on the geometry of the nuclear potential, which introduces additional, usually not considered, uncertainties in determination Γ_p from mirror symmetry. Therefore, we can expect differences in Γ_p determined by traditional Coulomb penetrability method and the method of Eq. (19) used here. We believe that a systematic comparison between

the two methods should be a subject of a separate paper. We just note that the width $\Gamma_p(l = 0) = 2.5 \times 10^{-8}$ eV of the $E_R = 127$ keV resonance in ²⁷Si obtained in Ref. [9] is about 3 times smaller than the values obtained in this paper while the $\Gamma_p = 5.1 \times 10^{-5}$ eV width for $E_R = 188$ keV resonance in ²⁷Si is similar to our results. For ⁵⁷Cu our Γ_p widths are about 100% and 40% larger than the $\Gamma_p = 5.7 \times 10^{-12}$ eV and 1.9×10^{-7} eV values obtained in Ref. [33] for $E_R = 336$ and 416 KeV resonances, respectively.

Finally, we have to comment on the determination of Γ_p from total (d, p) cross sections σ_t . We find that at $E_d = 12$ MeV the calculated total cross sections are not very sensitive to changes in r_0 , which suggests that peripherality of these reactions is lost, but offers an opportunity of determining the spectroscopic factors. The ANC's C_n^2 obtained from total cross sections could have large uncertainties, between 30 to 100%, being either comparable to or even larger than those due to the I3B effects. At $E_d = 60$ MeV the situation is different. Apart from ²⁷Al(7806) with $l = 0$ and ⁵⁷Ni(2577) cases, the ratio σ_t/b^2 , where b is the single-particle ANC, changes significantly with r_0 , indicating that peripherality is also lost at higher energies, as expected. At the same time σ_t also becomes r_0 -dependent, inducing large uncertainties in the spectroscopic factors as well. Once again, these uncertainties can be comparable to those originating from introducing I3B effects. A special case is ²⁷Al(7806) with $l = 0$ and ⁵⁷Ni(2577) cases, where changing r_0 within the interval of the most probable values, between 1.15 and 1.35 fm, results in a 3% change in σ_t/b^2 , with respect to the average value. This is sufficient to deduce C_n^2 for ⁵⁷Ni(2577), where only one l -value contributes to the total cross section. In this case, using $\sigma_t = 1.24$ mb for ⁵⁶Ni(d, p)⁵⁷Ni(2577) reaction measured at $E_d = 64$ MeV we obtain $\Gamma_p = 2.68$ eV, which is about 5 times larger than the 0.53 eV value obtained via Coulomb-barrier penetrability method, with uncertainties due to I3B effects being 6%–16%. For ²⁷Al(7806) the ANC's and the corresponding Γ_p cannot be determined since two unknown values need to be determined from only one experimental observable.

VII. CONCLUSIONS

We have presented calculations for cross sections of several (d, p) reactions populating excited states in ²⁷Al, ³¹P, ³⁵Cl, and ⁵⁷Ni, which are mirror analogs of important resonances

contributing to nucleosynthesis in various stellar environments via rp process. The main aim of these calculations was to quantify model uncertainties of the widely used ADWA arising due to projecting target excitations out, which affects two-body nucleon optical potentials in the $A + n + p$ three-body system and induces multiple-scattering terms in the three-body optical potential. Within the ADWA, these effects are accounted for by (a) evaluating the n - A and p - A optical potentials at energy shifted with respect to the $E_d/2$ value by half the n - p kinetic energy within the short range of V_{np} , and (b) doubling their imaginary parts. These corrections are introduced into two different nucleon optical potentials, the nonlocal energy-dependent potential GRZ, and the local global potential KD03, treating the latter in two different ways. The calculations were carried out at two typical energies, available at radioactive beam facilities, that have been already used for indirect study of astrophysically relevant reactions.

The shift of energy at which optical potentials should be evaluated in ADWA strongly depends on the choice of the deuteron model and this can significantly affect the (d, p) cross sections. The strong sensitivity to the deuteron model arises due to the existence of a deuteron d -wave state that contributes about 40% to the n - p potential-energy matrix element. Introducing I3B effects by doubling the imaginary part of the optical potentials reduce dependence on deuteron model choice. Choosing the s -wave Hulthén model we reduce the contribution from high n - p momenta along with contributions from nonadiabatic effects.

With the chosen deuteron model, including the three-body nature of the optical potentials in the $A + n + p$ system at a typical deuteron energy of $E_d = 12$ MeV does not change the shape of the angular distributions significantly with respect to predictions of the standard ADWA, resulting in a renormalization of the cross sections. This renormalization depends on the choice of optical potential being distinct for nonlocal and local ones. For nonlocal potentials, the I3B effects reduce the cross sections by up to 40% for ^{26}Al , ^{30}P , and ^{34}Cl targets, while for ^{56}Ni this reduction does not exceed 20%. For local potentials the change likewise does not exceed 20%, but can go either way, increasing or decreasing the cross sections. Two different ways of applying I3B effects in local potentials, either directly or to restored nonlocal equivalent, give very similar results. The total cross sections have larger model uncertainties, especially at higher deuteron energies. While at $E_d = 12$ MeV they do not exceed 35%, being in most cases within 10%–20%. At $E_d = 60$ MeV this uncertainty can

be as high as 100%, causing changes both ways, increasing or decreasing. These uncertainties will directly propagate to corresponding uncertainties in the widths of astrophysically relevant resonances and the associated proton capture reaction rates.

Current estimates of three-body effects in the optical potential of the $A + n + p$ system, arising from projecting out target excitations, are based on the ADWA. It is important to understand how they may change beyond the adiabatic assumptions. The only attempt to do this has been carried out using Faddeev equations with excited states, but neglecting the many-body nature of the target. Similar to our findings, treating the energy dependence of the optical potentials explicitly by adjusting two-body Faddeev T matrices increases the (d, p) cross sections requiring three-body optical potential that provides increasing absorption [36]. This is qualitatively the same effect as the one considered here. It is important to extend the three-body optical potential study to many-body systems beyond the adiabatic approximation. This will help to build more accurate models that will help to extract reliable spectroscopic information from (d, p) reactions for various applications, including understanding of stellar nucleosynthesis.

Finally, we would like to mention that, in addition to three-body potential effects induced by projecting out target excitations, there should exist a contribution to the three-body Hamiltonian that arises due to three-nucleon interactions between n , p and individual nucleons in the target [37]. This contribution depends on the choice of target, deuteron incident energy, binding energy of the state populated by the transferred neutron, and its orbital momentum. The three-nucleon interaction also introduces additional term into (d, p) T matrix [38]. These effects can introduce further model uncertainty to (d, p) cross sections, which will affect the spectroscopic information obtained from them. More work is needed to clarify their role.

Note added in proof. Our paper does not address the question of antisymmetrization. Nevertheless, the recent paper by Johnson in [39] provides a firm basis from an antisymmetrized many-body point of view for the three-body force effects calculated both in [4] and here.

ACKNOWLEDGMENTS

This work was supported by the United Kingdom Science and Technology Facilities Council (STFC) under Grant No. ST/L005743/1.

-
- [1] N. K. Timofeyuk, R. C. Johnson, and A. M. Mukhamedzhanov, *Phys. Rev. Lett.* **91**, 232501 (2003).
 - [2] R. C. Johnson and P. C. Tandy, *Nucl. Phys. A* **235**, 56 (1974).
 - [3] R. C. Johnson and N. K. Timofeyuk, *Phys. Rev. C* **89**, 024605 (2014).
 - [4] M. J. Dinmore, N. K. Timofeyuk, J. S. Al-Khalili, and R. C. Johnson, *Phys. Rev. C* **99**, 064612 (2019).
 - [5] C. Mahaux and R. Sartor, *Nucl. Phys. A* **484**, 205 (1988).
 - [6] S. J. Waldecker and N. K. Timofeyuk, *Phys. Rev. C* **94**, 034609 (2016).
 - [7] G. Lotay, P. J. Woods, D. Seweryniak, M. P. Carpenter, R. V. F. Janssens, and S. Zhu, *Phys. Rev. C* **80**, 055802 (2009).
 - [8] G. Lotay *et al.*, *Eur. Phys. J. A* **56**, 3 (2020).
 - [9] V. Margerin *et al.*, *Phys. Rev. Lett.* **115**, 062701 (2015).
 - [10] A. Kankainen *et al.*, *Eur. Phys. J. A* **52**, 1 (2016).
 - [11] J. Fallis *et al.*, *Phys. Rev. C* **88**, 045801 (2013).
 - [12] C. Iliadis *et al.*, *Astrophys. J., Suppl. Ser.* **142**, 105 (2002).

- [13] A. Kankainen *et al.*, *Phys. Lett. B* **769**, 549 (2017).
- [14] J. Jose *et al.*, *Astrophys. J.* **612**, 414 (2004).
- [15] C. Fry *et al.*, *Phys. Rev. C* **91**, 015803 (2015).
- [16] A. E. Champagne and M. Wiescher, *Annu. Rev. Nucl. Part. Sci.* **42**, 39 (1992).
- [17] J. W. Truran, *et al.*, *J. Phys.: Conf. Ser.* **337**, 012040 (2012).
- [18] K. E. Rehm *et al.*, *Phys. Rev. Lett.* **80**, 676 (1998).
- [19] J. A. Tostevin, University of Surrey version of the code TWOFNR (M. Toyama, M. Igarashi, and N. Kishida) and code FRONT (private communication).
- [20] G. W. Bailey, N. K. Timofeyuk, and J. A. Tostevin, *Phys. Rev. C* **95**, 024603 (2017).
- [21] L. Hulthén and M. Sugawara, *The Two-Nucleon Problem* (Springer-Verlag, Berlin, 1957).
- [22] R. B. Wiringa, V. G. J. Stoks, and R. Schiavilla, *Phys. Rev. C* **51**, 38 (1995).
- [23] R. Machleidt, *Phys. Rev. C* **63**, 024001 (2001).
- [24] E. Epelbaum, H. Krebs, and U.-G. Meißner, *Phys. Rev. Lett.* **115**, 122301 (2015).
- [25] M. M. Giannini, G. Ricco, and A. Zucchiatti, *Ann. Phys. (NY)* **124**, 208 (1980).
- [26] G. W. Bailey, N. K. Timofeyuk, and J. A. Tostevin, *Phys. Rev. Lett.* **117**, 162502 (2016).
- [27] A. Deltuva, *Phys. Rev. C* **98**, 021603(R) (2018).
- [28] M. Gómez-Ramos and N. K. Timofeyuk, *Phys. Rev. C* **98**, 011601(R) (2018).
- [29] A. J. Koning and J. P. Delaroche, *Nucl. Phys. A* **713**, 231 (2008).
- [30] F. Perey and B. Buck, *Nucl. Phys.* **32**, 353 (1962).
- [31] N. K. Timofeyuk and R. C. Johnson, *Prog. Part. Nucl. Phys.* **111**, 103738 (2020).
- [32] N. K. Timofeyuk and R. C. Johnson, *Phys. Rev. C* **87**, 064610 (2013).
- [33] D. Kahl *et al.*, *Phys. Lett. B* **797**, 134803 (2019).
- [34] S. Hallam *et al.*, *Phys. Rev. Lett.* **126**, 042701 (2021).
- [35] A. M. Mukhamedzhanov, *Phys. Rev. C* **99**, 024311 (2019).
- [36] A. Deltuva, D. Jurciukonis, and E. Norvaisas, *Phys. Lett. B* **769**, 202 (2017).
- [37] N. K. Timofeyuk, M. J. Dinmore, and J. S. Al-Khalili, *Phys. Rev. C* **102**, 064616 (2020).
- [38] N. K. Timofeyuk, *Phys. Rev. C* **97**, 054601 (2018).
- [39] R. C. Johnson, *Phys. Rev. C* **104**, 024612 (2021).